A New Cold Stream near the Southern Galactic Pole

Yong Yang[1,2] , Jing-Kun Zhao[1,3] , Xiang-Xiang Xue[1] , Xian-Hao Ye[1,2] , and Gang Zhao[1,2]

[1] CAS Key Laboratory of Optical Astronomy, National Astronomical Observatories, Chinese Academy of Sciences, Beijing 100101, People's Republic of China
zjk@bao.ac.cn
[2] School of Astronomy and Space Science, University of Chinese Academy of Sciences, Beijing 100049, People's Republic of China
[3] School of Physics and Astronomy, China West Normal University, Nanchong 637009, People's Republic of China

Abstract

We report the discovery of a cold stream near the southern Galactic pole (dubbed as SGP-S) detected in Gaia Early Data Release 3. The stream is at a heliocentric distance of $\sim$9.5 kpc and spans nearly $58°$ by $0°\!.6$ on sky. The color–magnitude diagram of SGP-S indicates an old and metal-poor (age $\sim$12 Gyr, [M/H] ~ -2.0 dex) stellar population. The stream's surface brightness reaches an exceedingly low level of $\Sigma_G \simeq 36.2$ mag arcsec^{-2}. Neither extant globular clusters nor other known streams are associated with SGP-S.

Unified Astronomy Thesaurus concepts: Milky Way Galaxy (1054); Milky Way stellar halo (1060); Tidal tails (1701); Globular star clusters (656)

1. Introduction

An increasing amount of data from revolutionary surveys are revealing that the Milky Way is full of substructures, either in the disk (e.g., Zhao et al. 2009; Liang et al. 2017; Ramos et al. 2018; Zhao et al. 2018; Antoja et al. 2018; Ye et al. 2021; Re Fiorentin et al. 2021; Yang et al. 2021; Zhao & Chen 2021), or in the halo (e.g., Ibata et al. 1994; Newberg et al. 2002, 2009; Law & Majewski 2010; Helmi et al. 2018; Zhao et al. 2020). Among those substructures, dynamically cold streams, which are usually related to globular clusters (GCs), play an important role (e.g., Grillmair & Johnson 2006; Grillmair & Dionatos 2006; Odenkirchen et al. 2009; Bonaca et al. 2012; Koposov et al. 2014). It has been proven that cold streams are powerful tools in constraining the Galactic potential and studying the formation history of the stellar halo (Koposov et al. 2010; Lux et al. 2013; Bovy et al. 2016; Malhan & Ibata 2019; Ibata et al. 2021; Yang et al. 2022).

In this Letter, we report the discovery of a new cold stream near the southern Galactic pole, which we designate SGP-S. The stream is exposed by weighting stars in a color–magnitude diagram (CMD) and proper motions (PMs) simultaneously using Gaia Early Data Release 3 (EDR3) (Gaia Collaboration et al. 2021; Lindegren et al. 2021; Riello et al. 2021). Section 2 describes the detecting strategy, and Section 3 characterizes the stream. A conclusion is given in Section 4.

2. Weighting Stars

We first need to clarify that SGP-S was detected by chance while examining the existence of GC NGC 5824's leading tail. Specifically, Bonaca et al. (2021) and Li et al. (2022) pointed out that the Triangulum (Bonaca et al. 2012) and Turbio (Shipp et al. 2018) streams could be associated with NGC 5824. Motivated by this, we tried to search for other stream segments along its leading tail using a modified matched-filter technique from Grillmair (2019). The technique weighted stars using their color differences from the cluster's locus in CMD. These

weights are further scaled based on stars' departures from PMs of the NGC 5824 model stream. By applying the method, we accidentally found the signature of SGP-S.

After some experiments, we optimize the choices of the filters and present details of the detection as follows. Stars from Gaia EDR3 within a sky box of $-20° < \alpha < 20°$ and $-90° < \delta < 40°$ are retrieved. As Riello et al. (2021) pointed out, for the source without a measured ν_{eff} (effective wavenumber) used in determining the G-band flux, a default ν_{eff} is adopted; this will lead to a systematic effect in G-band photometry. In addition, Riello et al. (2021) introduced the corrected BP and RP flux excess factor C^* to identify sources for which the G-band photometry and BP and RP photometry are not consistent. We correct the G magnitude and calculate C^* for our sample according to Riello et al.'s Tables 2 and 5. In order to ensure good astrometric and photometric solutions, only stars with `ruwe` < 1.4 and $|C^*| < 3\sigma_{C^*}$ (see Section 9.4 in Riello et al. 2021) are retained.
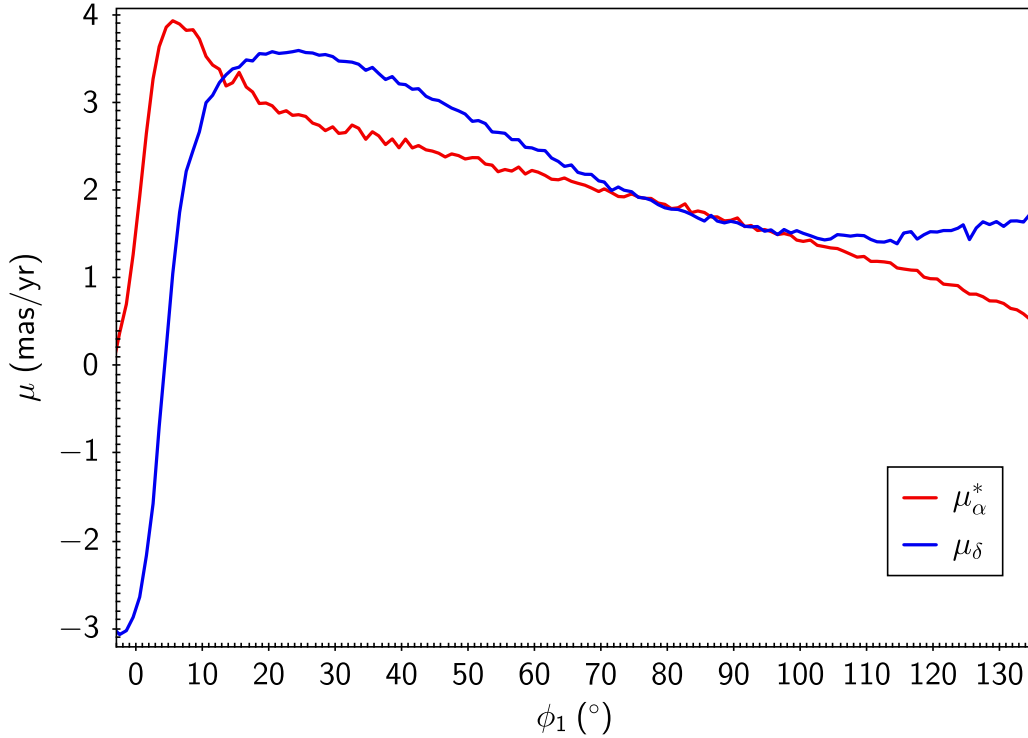
In the CMD, we use a set of stellar tracks extracted from the Padova database (Bressan et al. 2012) at different distances as the filters. The isochrone grid explored here covers a metallicity range of $-2.2 \leqslant$ [M/H] $\leqslant -1.2$ and an age range of $10 \leqslant$ Age $\leqslant 13$ with 0.1 dex and 1 Gyr spacing, along with a distance modulus (DM) varying from 14 to 17 with a step of 0.1 mag. Individual stars are assigned weights based on their color differences from a given isochrone filter, assuming a Gaussian error distribution:

$$w_{\mathrm{CMD}} = \frac{1}{\sqrt{2\pi}\,\sigma_{\mathrm{color}}} \exp\left[-\frac{1}{2}\left(\frac{\mathrm{color} - \mathrm{color}_0}{\sigma_{\mathrm{color}}}\right)^2\right]. \quad (1)$$

Here color and σ_{color} denote BP – RP and corresponding errors. σ_{color} is simply calculated through $\sqrt{\sigma_{\mathrm{BP}}^2 + \sigma_{\mathrm{RP}}^2}$, where σ_{BP} and σ_{RP} are obtained with a propagation of flux errors (see the CDS website[4]). color_0 is determined by the isochrone at a given G magnitude of a star. All stars have been extinction-corrected using the Schlegel et al. (1998) maps as recalibrated by Schlafly & Finkbeiner (2011) with $RV = 3.1$, assuming

---

[4] https://vizier.u-strasbg.fr/viz-bin/VizieR-n?-source=METAnot&catid=1350&notid=63&-out=text

Figure 1. The PM filters used to weight stars with Equation (2). ϕ_1 is the longitude in a rotated frame with a pole of ($\alpha = 270°$, $\delta = 0°$). The red line denotes the μ_α^* medians of NGC 5824 model stream particles in each ϕ_1 bin with a bin width of 1°.1 mas yr^{-1} is further added to their μ_δ medians; it is shown with the blue line.

$A_G/A_V = 0.83627$, $A_{BP}/A_V = 1.08337$, and $A_{RP}/A_V = 0.63439$.[5]

In terms of PMs, weights are computed as

$$w_{\text{PMs}} = \frac{1}{2\pi\sigma_{\mu_\alpha^*}\sigma_{\mu_\delta}} \exp\left\{-\frac{1}{2}\left[\left(\frac{\mu_\alpha^* - \mu_{\alpha,0}^*}{\sigma_{\mu_\alpha^*}}\right)^2 + \left(\frac{\mu_\delta - \mu_{\delta,0}}{\sigma_{\mu_\delta}}\right)^2\right]\right\}. \quad (2)$$

Here, μ_α^*, μ_δ, $\sigma_{\mu_\alpha^*}$, and σ_{μ_δ} are measured PMs and corresponding errors. $\mu_{\alpha,0}^*$ and $\mu_{\delta,0}$ are the components of PMs predicted at each star's ϕ_1 based on the run in Figure 1. For easier data processing and clearer presentation of results, we rotate celestial coordinates such that the point ($\alpha = 270°$, $\delta = 0°$) is the pole. Hence, ϕ_1 here, which is the new longitude, corresponds to δ but starts at $\delta = -90°$ and increases along $\alpha = 0°$. The red and blue tracks come from the model stream of NGC 5824. The way of generating the model stream follows closely that of Yang et al. (2022) as applied to NGC 5466. Under a static Milky Way potential plus a moving Large Magellanic Cloud (LMC), GC NGC 5824 is initialized 2 Gyr ago and integrated forward from then on, releasing particles in both leading and trailing directions at Lagrange points (Gibbons et al. 2014; Erkal et al. 2019). The resulting stream particles are divided into ϕ_1 bins (bin width = 1°), and medians of PMs in each bin are calculated, by which the PM tracks of Figure 1 are obtained. We further add 1 mas yr^{-1} to the whole

μ_δ because such a filter is a closer estimate of the μ_δ trend of SGP-S and gives stronger signals (see below).

Finally, the stars' weights are obtained by multiplying w_{CMD} and w_{PMs}, and then summed in sky pixels to expose structures.

3. The SGP-S

A weighted sky map is obtained as shown in the middle panel of Figure 2. Here the isochrone filter of Age = 12 Gyr, [M/H] = −2.0 dex, and DM = 14.9 mag is used during weighting stars in the CMD, which is the best-fit result that presents the strongest stream signal.[6] The sky pixel width is 0°.2 and the map is smoothed with a Gaussian kernel of $\sigma = 0°.3$. The stretch is logarithmic, with brighter areas corresponding to higher weight regions. The blue arrow points to the Small Magellanic Cloud (SMC). On the upper and lower panels, we further plot the dust extinction map extracted from Schlegel et al. (1998) and Gaia's scanning pattern covered by the EDR3, respectively, with higher values represented by darker colors. The red dashed line of the three panels indicates the trajectory of SGP-S fitted by a polynomial of

$$\phi_2 = 1.41834461 \times 10^{-3}\phi_1^2 - 0.132161401\phi_1 - 2.71971339. \quad (3)$$

From the matched-filter map, the signature of SGP-S is quite obvious, starting at $\phi_1 \simeq 29°$ and ending at $\phi_1 \simeq 87°$. Besides, there are several random noises appearing above and to the right of the stream. They do not represent physical overdensities but are caused by some field stars distributed coincidentally close to our CMD and PM filters because more stars populate the higher ϕ_1 (near the disk) and higher ϕ_2 (see

---

[5] These extinction ratios are listed on the Padova model site: http://stev.oapd.inaf.it/cgi-bin/cmd.

[6] We measure the stream's strength through the total weights between $-6°.2 < \phi_2 < -4°.8$ in Figure 3.
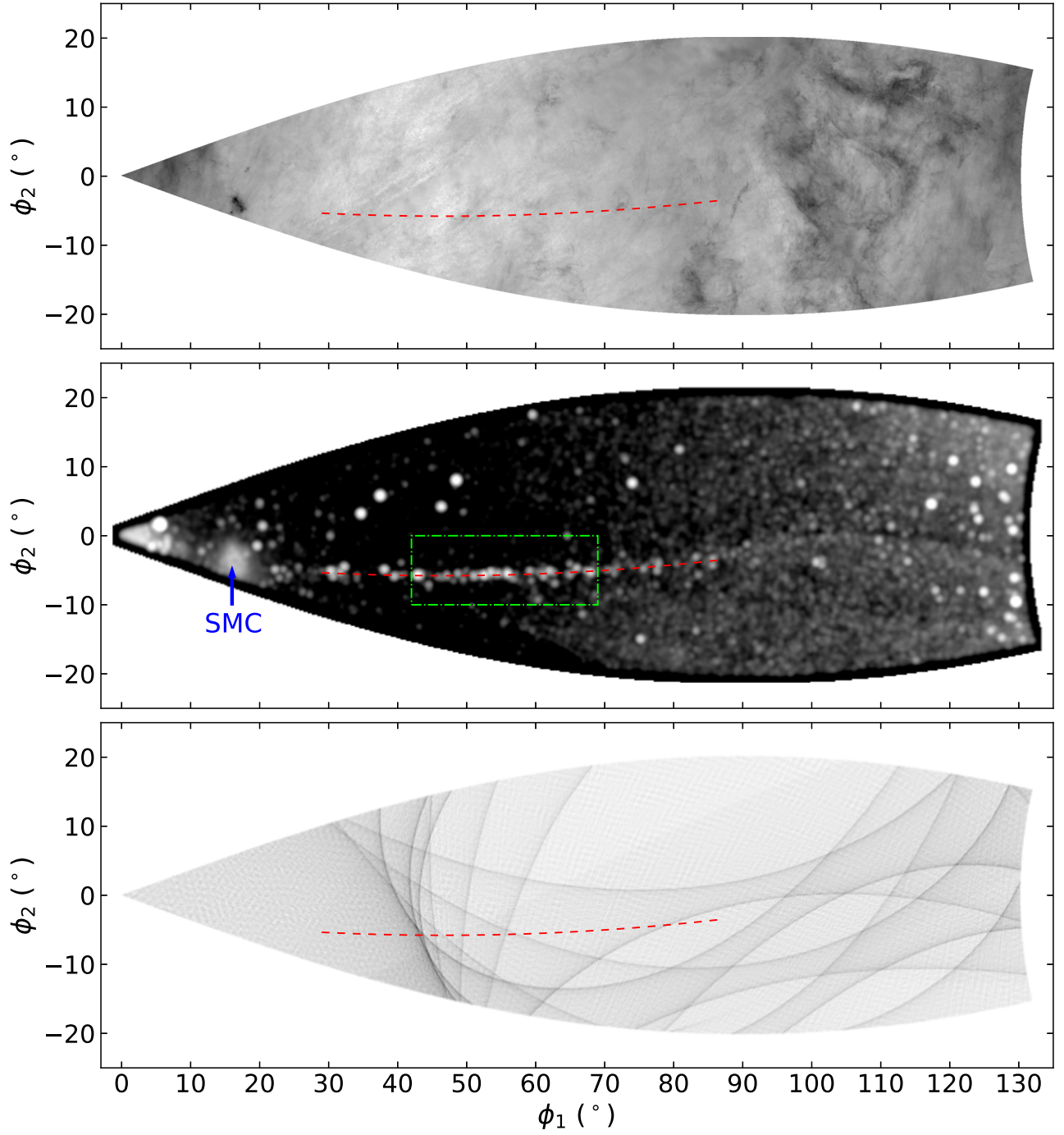
Figure 2. The upper and lower panels present the dust extinction map extracted from Schlegel et al. (1998) and Gaia's scanning pattern covered by the EDR3, respectively. The middle panel presents the weighted sky map. The blue arrow points to the SMC. Stars within the green rectangle are used to create the lateral profile of SGP-S. The red dashed line of the three panels indicates the trajectory of the stream.

Figure 3) sides. Using the other two panels, we can verify that the stream does not follow any structures in the interstellar extinction and is not aligned with any features in Gaia's scanning pattern. The trajectory in the ICRS frame can be well described with a third-order polynomial:

$$\alpha = -2.44373567 \times 10^{-5}\delta^3 - 1.62880413 \times 10^{-3}\delta^2 \\ - 0.138532434\delta + 3.04632126, \quad (4)$$

where $-61° < \delta < -3°$.

To estimate the stream's width, we select stars within a box of $42° < \phi_1 < 69°$ and $-10° < \phi_2 < 0°$ (green rectangle of

Figure 2), in which the stream is almost parallel to the ϕ_1-axis. We then sum these weights in each ϕ_2 bin (bin width = 0°.15) to create a one-dimensional stream profile as shown with the red solid line in Figure 3. The stream is almost enclosed within $-6°.2 < \phi_2 < -4°.8$, and its peak is 41σ above the background noise outside this range. From the profile, we find an estimate of its width (FWHM) to be $\sim 0°.6$.

Furthermore, we create the lateral profile of the star's number in the same way and overplot it with the blue dashed line in Figure 3. There is a gradient in the distribution of stars along ϕ_2, with more stars populated at higher ϕ_2. It can be concluded that the stream

3
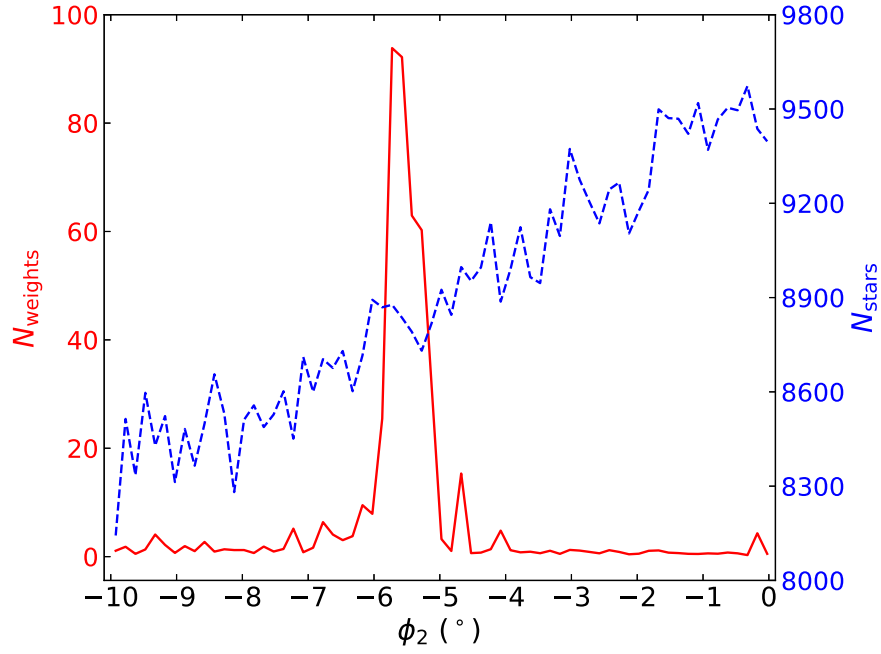
Figure 3. The lateral distributions along ϕ_2 for weighted (red solid) and unweighted (blue dashed) numbers of stars within the green rectangle of Figure 2.
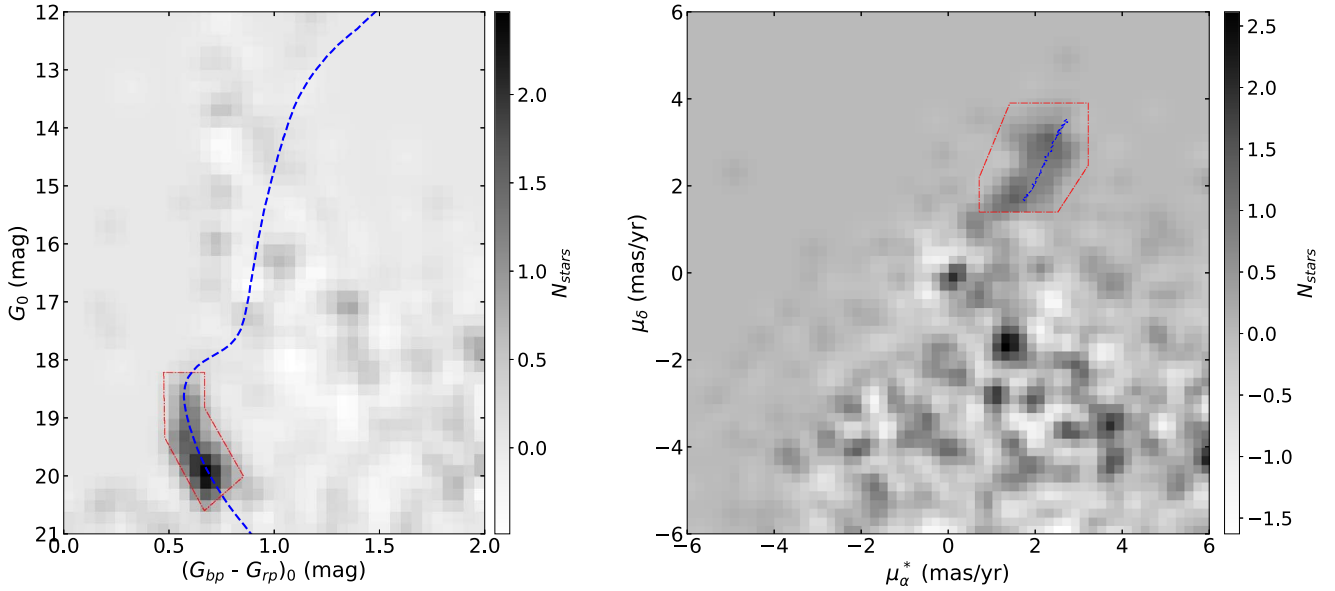
Figure 4. The left panel is a 2D histogram of stars in CMD with PMs selected and background subtracted. The blue dashed line represents the best-fit isochrone with Age = 12 Gyr and [M/H] = −2.0 dex at DM = 14.9 mag. The right panel is a 2D histogram of PMs after CMD selection and background subtraction. The filters of Figure 1 within $29° < \phi_1 < 87°$ are overplotted in the blue line. Both of the diagrams are smoothed with a 2D Gaussian kernel of $\sigma = 1$ pixel. The red polygons represent the CMD and PM selections applied to the stream and off-stream regions.

signature is not caused by contamination of the Milky Way's field population. Otherwise, it is more likely to detect strong signals close to the $\phi_2 = 0°$ side. The same analysis is performed for other stream segments, and similar profiles for weighted and unweighted numbers of stars can be found.

3.1. CMD and PMs

We display a background-subtracted binned CMD for the stream in the left panel of Figure 4. The stream region is defined as the area around the trajectory (Equation (3)) ±0°.3 in ϕ_2, given the derived width of 0.6°. The background is estimated by averaging two off-stream regions parallel to the

stream obtained by moving the stream region along the ϕ_2-axis by ±2° to eliminate the effect of the gradient. Before the background subtraction, a PM selection is applied to both the stream and off-stream regions as illustrated by the red polygon in the right panel of Figure 4, which corresponds to the stream's distribution in PM space (see below). We emphasize that this is a subtraction of star numbers, not weighted counts.

The CMD bin size is 0.05 mag in color and 0.2 mag in G magnitude. The diagram is smoothed with a 2D Gaussian kernel of $\sigma = 1$ pixel. The blue dashed line represents the best-fit isochrone with Age = 12 Gyr and [M/H] = −2.0 dex at DM = 14.9 mag. After the PM selection and background subtraction, the stream's main sequence along with its turnoff
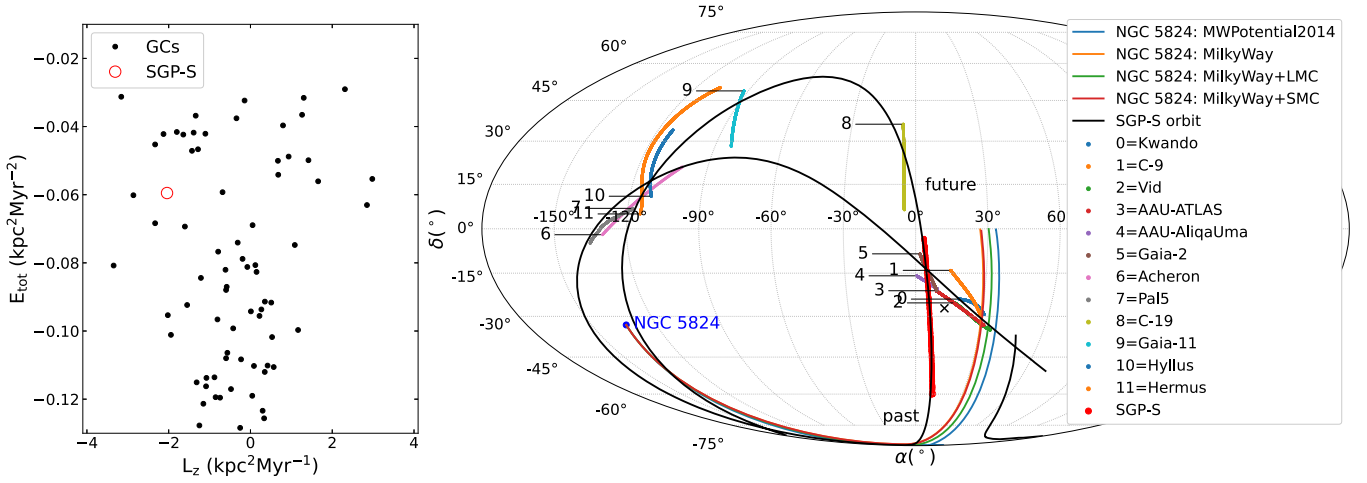
Figure 5. The left panel displays GCs (black points) and SGP-S (red circle) in angular momenta and energy space. The right panel presents projections of streams and orbits in ICRS frame. The red track and black line indicate SGP-S and its best-fit orbit. Colored lines represent orbital paths for GC NGC 5824 integrated in different potential models. Numbered tracks represent 12 known streams obtained from Mateu (2022). The black cross denotes the southern Galactic pole.

is clearly seen and has a good match with the isochrone. The DM 14.9 mag corresponds to a heliocentric distance of ∼9.5 kpc. Considering the width of 0°.6, the physical width of SGP-S is about 100 pc, comparable to dynamically cold streams with GC origins such as Pal 5 (120 pc; Odenkirchen et al. 2003), Triangulum (75 pc; Bonaca et al. 2012), ATLAS (90 pc; Koposov et al. 2014), and Molonglo (128 pc; Shipp et al. 2018).

In the right panel of Figure 4, we present a 2D histogram of PMs. Similarly, before the subtraction between the stream region and the mean of the off-stream regions, a CMD selection is applied to them as shown by the red polygon in the left panel. The diagram with bin size $= 0.2$ mas yr^{-1} is also smoothed using a 2D Gaussian with $\sigma = 1$ pixel. The filters of Figure 1 within $29° < \phi_1 < 87°$ are overplotted in the blue dashed line. An overdensity at $\mu_\alpha^* \sim 2.0$ mas yr^{-1} and $\mu_\delta \sim 2.5$ mas yr^{-1} corresponding to the stream is discernible. We note that our PM filters happen to be a rough estimate of the stream's PMs. It is worth noting that the PM filters are necessary to expose SGP-S because the signals are indistinguishable when using the CMD filter alone, and the PM filters assign rather low weights to most of the field stars so that the stream can be discerned.

The stream's surface density and brightness are further estimated. There are a total of 106 stars within the PM polygon after the background subtraction. This serves as an estimate of the number of the stream stars located in a $58° \times 0°.6$ region observed by Gaia. Thus the surface density is roughly 3 stars degree^{-2}. For all stars in the stream region, each one is assigned a weight by the matched-filter method and this allows us to select the most likely members of the stream based on the sort of weights. We adopt stars with weights >0.08 as the member candidates because the criterion leaves us 106 stars as well. By combining their individual G magnitudes, we get a surface brightness of SGP-S to be $\Sigma_G \simeq 36.2$ mag arcsec^{-2}, which is even darker than, for example, Phlegethon (34.3 mag arcsec^{-2}; Ibata et al. 2018) and the trailing tail of M5 (35 mag arcsec^{-2}; Grillmair 2019).

3.2. Association with GCs and Streams

We aim to fit an orbit to SGP-S so that we can investigate whether it is related to any GCs or known streams of the Milky Way. We assume a Galactic potential model of MWPotential2014 (Bovy 2015). The solar distance to the Galactic

center, circular velocity at the Sun, and solar velocities relative to the local standard of rest are set to 8 kpc, 220 km s^{-1} (Bovy et al. 2012), and (11.1, 12.24, and 7.25) km s^{-1} (Schönrich et al. 2010), respectively. The fitting parameters are position α, δ, heliocentric distance d, PMs μ_α^*, μ_δ, and radial velocity V_r. We chose to anchor the decl. at $\delta = -61°$, an endpoint of the stream, leaving other parameters free to be varied. In a Bayesian framework, sky positions and PMs of 106 member candidates are used to constrain the parameters and the fitted results can be derived from their marginalized posterior distributions through a Markov Chain Monte Carlo sampling. The best-fit parameters are $\alpha = 9.63^{+0.09}_{-0.09}°$, $d = 10.17^{+0.12}_{-0.12}$ kpc, $\mu_\alpha^* = 2.47^{+0.04}_{-0.04}$ mas yr^{-1}, $\mu_\delta = 3.53^{+0.07}_{-0.07}$ mas yr^{-1}, and $V_r = 34.06^{+3.64}_{-3.68}$ km s^{-1}.

We first examine possible connections between SGP-S and GCs by comparing their angular momenta L_z and energy E_{tot} as shown in the left panel of Figure 5. The positions and velocities of GCs are taken from Vasiliev & Baumgardt (2021). It can be seen that the stream does not lie close to any other GCs. We have further integrated orbits of all 160 GCs and then compared them to the trajectory of SGP-S but no consistent orbits are found. We consider that the progenitor for SGP-S might have been dissolved.

In the right panel, we present the trajectory of SGP-S (red track) along with its best-fit orbit (black line) integrated for ± 1 Gyr to the past and future. Its pericenter and apocenter are $R_{peri} = 10.5$ kpc and $R_{apo} = 9.6$ kpc, respectively. Since the detection is motivated by searching for GC NGC 5824's tidal debris, its orbital path is also overplotted for a comparison. We explore the cluster's orbits using four potential models. The first one is MWPotential2014 used in this work (blue line). The second one come from the static Milky Way potential as applied in Yang et al. (2022), which we refer to as MilkyWay (orange line). The other two potentials further contain the LMC (green line) or SMC (red line) components on the basis of MilkyWay, both of which are modeled using a Hernquist (1990) sphere with masses and scale sizes from El-Falou & Webb (2022). Apparently, although SGP-S is found coincidentally using the PMs of NGC 5824 model stream, they are completely separated on sky, even if variations and perturbations in potential models are taken into consideration.

Furthermore, 12 known streams nearly aligned with SGP-S's orbit on sky are also presented as marked in different numbers, which are obtained from (Mateu 2022, and references therein). Although some stream projections seem to fit the orbit well, they are actually not connected when considering additional criteria. Specifically, R_{peri} and R_{apo} values for Kwando (4.4, 26.4), C-19 (7.0, 27.4), Hermus (7.1, 17.2), and Hyllus (5.4, 18.6) kpc are inconsistent with those of SGP-S. The other streams are separated from the orbit in heliocentric distance: C-9 (8.1 versus 15.2),[7] Vid (24.5 versus 16.1), ATLAS (20.2 versus 15.3), Aliqa Uma (26.6 versus 12.1), Gaia-2 (7.0 versus 12.0), Acheron (3.6 versus 33.5), Pal 5 (21.2 versus 43.1), and Gaia-11 (12.4 versus 36.0) kpc. Hence, it is concluded that there is no favorable match to newly discovered SGP-S among known streams.

4. Conclusion

With revised photometry and astrometry from Gaia EDR3, we have discovered a new cold stream near the southern Galactic pole which we dub SGP-S. The stream is detected at a significance of 41σ through a modified matched-filter that assigns weights to stars in CMD and PMs simultaneously. The SGP-S is spanning $58°$ by $0°6$ on sky at 9.5 kpc away from the Sun. The best-fit isochrone indicates an old (~12 Gyr) and metal-poor (~-2.0 dex) stellar population. The stream has an extremely low surface brightness of $\Sigma_G \simeq 36.2$ mag arcsec^{-2}, with a density of about 3 stars degree^{-2}. Given the physical width to be 100 pc, we further explore the possibility of connections between SGP-S and extant GCs along with other narrow streams of the Milky Way and find that none of them has similar dynamical properties to the stream. Follow-up observations and studies might be able to uncover the origin of SGP-S.

ORCID iDs

Yong Yang ⓘ https://orcid.org/0000-0001-7609-1947
Jing-Kun Zhao ⓘ https://orcid.org/0000-0003-2868-8276
Xiang-Xiang Xue ⓘ https://orcid.org/0000-0002-0642-5689
Xian-Hao Ye ⓘ https://orcid.org/0000-0002-5805-8112
Gang Zhao ⓘ https://orcid.org/0000-0002-8980-945X

References

Antoja, T., Helmi, A., Romero-Gómez, M., et al. 2018, Natur, 561, 360
Bonaca, A., Geha, M., & Kallivayalil, N. 2012, ApJL, 760, L6
Bonaca, A., Naidu, R. P., Conroy, C., et al. 2021, ApJL, 909, L26
Bovy, J. 2015, ApJS, 216, 29
Bovy, J., Bahmanyar, A., Fritz, T. K., & Kallivayalil, N. 2016, ApJ, 833, 31
Bovy, J., Allende Prieto, C., Beers, T. C., et al. 2012, ApJ, 759, 131
Bressan, A., Marigo, P., Girardi, L., et al. 2012, MNRAS, 427, 127
El-Falou, N., & Webb, J. J. 2022, MNRAS, 510, 2437
Erkal, D., Belokurov, V., Laporte, C. F. P., et al. 2019, MNRAS, 487, 2685
Gaia Collaboration, Brown, A. G. A., Vallenari, A., et al. 2021, A&A, 649, A1
Gibbons, S. L. J., Belokurov, V., & Evans, N. W. 2014, MNRAS, 445, 3788
Grillmair, C. J. 2019, ApJ, 884, 174
Grillmair, C. J., & Dionatos, O. 2006, ApJL, 643, L17
Grillmair, C. J., & Johnson, R. 2006, ApJL, 639, L17
Helmi, A., Babusiaux, C., Koppelman, H. H., et al. 2018, Natur, 563, 85
Hernquist, L. 1990, ApJ, 356, 359
Ibata, R., Malhan, K., Martin, N., et al. 2021, ApJ, 914, 123
Ibata, R. A., Gilmore, G., & Irwin, M. J. 1994, Natur, 370, 194
Ibata, R. A., Malhan, K., Martin, N. F., & Starkenburg, E. 2018, ApJ, 865, 85
Koposov, S. E., Irwin, M., Belokurov, V., et al. 2014, MNRAS, 442, L85
Koposov, S. E., Rix, H.-W., & Hogg, D. W. 2010, ApJ, 712, 260
Law, D. R., & Majewski, S. R. 2010, ApJ, 714, 229
Li, T. S., Ji, A. P., Pace, A. B., et al. 2022, ApJ, 928, 30
Liang, X. L., Zhao, J. K., Oswalt, T. D., et al. 2017, ApJ, 844, 152
Lindegren, L., Klioner, S. A., Hernández, J., et al. 2021, A&A, 649, A2
Lux, H., Read, J. I., Lake, G., & Johnston, K. V. 2013, MNRAS, 436, 2386
Malhan, K., & Ibata, R. A. 2019, MNRAS, 486, 2995
Mateu, C. 2022, arXiv:2204.10326
Newberg, H. J., Yanny, B., & Willett, B. A. 2009, ApJL, 700, L61
Newberg, H. J., Yanny, B., Rockosi, C., et al. 2002, ApJ, 569, 245
Odenkirchen, M., Grebel, E. K., Kayser, A., Rix, H.-W., & Dehnen, W. 2009, AJ, 137, 3378
Odenkirchen, M., Grebel, E. K., Dehnen, W., et al. 2003, AJ, 126, 2385
Ramos, P., Antoja, T., & Figueras, F. 2018, A&A, 619, A72
Re Fiorentin, P., Spagna, A., Lattanzi, M. G., & Cignoni, M. 2021, ApJL, 907, L16
Riello, M., De Angeli, F., Evans, D. W., et al. 2021, A&A, 649, A3
Schlafly, E. F., & Finkbeiner, D. P. 2011, ApJ, 737, 103
Schlegel, D. J., Finkbeiner, D. P., & Davis, M. 1998, ApJ, 500, 525
Schönrich, R., Binney, J., & Dehnen, W. 2010, MNRAS, 403, 1829
Shipp, N., Drlica-Wagner, A., Balbinot, E., et al. 2018, ApJ, 862, 114
Vasiliev, E., & Baumgardt, H. 2021, MNRAS, 505, 5978
Yang, Y., Zhao, J., Zhang, J., Ye, X., & Zhao, G. 2021, ApJ, 922, 105
Yang, Y., Zhao, J.-K., Ishigaki, M. N., et al. 2022, MNRAS, 513, 853
Ye, X., Zhao, J., Zhang, J., Yang, Y., & Zhao, G. 2021, AJ, 162, 171
Zhao, G., & Chen, Y. 2021, SCPMA, 64, 239562
Zhao, J., Zhao, G., & Chen, Y. 2009, ApJL, 692, L113
Zhao, J. K., Zhao, G., Aoki, W., et al. 2018, ApJ, 868, 105
Zhao, J. K., Ye, X. H., Wu, H., et al. 2020, ApJ, 904, 61

---

[7] The median distance of streams versus the orbital distance of SGP-S.